JOURNAL OF GEOPHYSICAL RESEARCH, VOL. 105, NO. E4, PAGES 9521–9537, APRIL 25, 2000

Thermal tides and stationary waves on Mars as revealed by Mars Global Surveyor thermal emission spectrometer

Don Banfield and Barney Conrath
Department of Astronomy, Cornell University, Ithaca, New York

John C. Pearl and Michael D. Smith
NASA Goddard Space Flight Center, Greenbelt, Maryland

Phil Christensen
Department of Geology, Arizona State University, Tempe

Abstract. Atmospheric temperature retrievals from thermal emission spectrometer (TES) observed radiances make possible the most complete separation of the constituent wave modes evident in Mars atmosphere to date. We use all of the data from the first aerobraking period as well as the science phasing orbits, which affords good sampling of the diurnal tides and stationary waves. TES retrievals of atmospheric temperature on a grid of pressure levels are the fundamental data set in this study. We then fit this data to selected Fourier modes in longitude and time for altitude, latitude, and L_s bins. From this we have identified the amplitudes and phases of the diurnal and semidiurnal tides, the first few (gravest) stationary waves, and a few modes which arise because of couplings between sun-fixed tides and topography. We also retrieve estimates of the zonal and time of day mean temperature meridional cross sections and their rates of change. The zonal and time of day mean temperature meridional cross sections agree with those of *Conrath et al.* [this issue] to within 1 K where we can reliably retrieve this mode (90°S to ~20°S). Heating rates of up to 2.4 K/sol were observed around three scale heights above 60°S-90°S during the $L_s = 310° - 320°$ dust storm. Diurnal tide amplitudes of greater than 8 K were observed during the Noachis and $L_s = 310° - 320°$ dust storms. From $L_s = 255° - 285°$ an unexplained phase reversal at two scale heights was observed in the diurnal tide from 60°S-80°S. Convective penetration above the unstable boundary layer may explain anomalous (180°out of phase with the sun) diurnal tide phases between 0.5 and one scale height above the subsolar point. Semidiurnal tides are of order 2 K throughout the southern extratropics. A stationary mode of wavenumber one was observed with amplitude 1-4 K in the southern extratropics. Topographically coupled tidal modes were also quantified.

1. Introduction

Mars Global Surveyor's (MGS) thermal emission spectrometer (TES) has been used to retrieve atmospheric temperatures as the spacecraft scanned different locations on the planet [*Conrath et al.*, this issue]. Because the spacecraft was inserted slowly into its mapping orbit using aerobraking, MGS and TES had a long period of time to observe many different combinations of time of day, latitude, and longitude. The result is that this subset of data (from the first aerobraking period (AB1) and science phasing orbits (SPO) of the mission) is the best yet for discerning the different wave modes that exist in Mars atmosphere. That is the focus of this work.

Waves in Mars' atmosphere have been studied from orbit since Mariner 9 first took measurements that revealed the atmospheric temperature. The diurnal thermal tide was easily identified in these data because of its large amplitude [e.g., *Pirraglia and Conrath*, 1974]. *Conrath* [1981] analyzed a subset of the data (northern winter midlatitudes) and found wave-like perturbations but could not determine specifically what type of wave it was because of the spacecraft's sampling pattern. He found it consistent with either a traveling baroclinic

Paper number 1999JE001161.
0148-0227/00/1999JE001161$09.00

wave or a stationary wave of wavenumber 2. *Banfield et al.* [1996] identified what appeared to be thermal tides and stationary waves in infrared thermal mapper (IRTM) T15 data, although recent work suggests that the data and that portion of their work may have been corrupted by surface radiance [*Wilson and Richardson*, 2000].

These studies of the waves present in Mars atmosphere have put useful but limited constraints on atmospheric models. *Nayvelt et al.* [1997] tried to explain some of the observed surface streaks in terms of stationary wave observations. Much work has been done examining the connection between atmospheric dust opacity and the thermal tides [e.g., *Leovy and Zurek*, 1979]. However, observations of global waves are scarce, a fact which we hope to partially remedy with this work. The impact of these results will lead to more faithful models and a better understanding of the phenomena in Mars' atmosphere.

In this work, we make a distinction between waves which are highly predictable, either by being fixed in space or forced directly by the sun, and those waves which are much less predictable and travel at all manner of speeds. The highly predictable waves we consider part of the climatology, while the other waves are what we loosely call "weather." In this work, we focus on the predictable waves, leaving the "weather" for a later work. In section 2, we discuss which subset of the data we have examined and why and the properties of the TES instrument and its atmospheric retrievals. Following that we define the wave modes that we solve for and then go on to describe the methods we used to estimate amplitudes and phases. Next we present some of our results. Finally, we conclude with a discussion of some possible implications of these results and a summary.

2. Data Set

2.1. Orbits and Coverage

The data we use in this study are the atmospheric temperature retrievals from the MGS spacecraft's TES instrument from the AB1 and SPO phases of the mission, that is, before the mapping phase. After entering the polar mapping orbit, TES was restricted to observations only at certain fixed times of day. Although favored for mapping purposes, this orbit is not well suited for sampling time of day variations. Because the diurnal variations typically dominate, it is easy for them to alias into other modes if they are not well observed. It may prove possible to use the horizon sensors on the spacecraft to infer the time of day variations during the mapping phase of the mission, but that approach has not yet been fully tested (T.Z. Martin, private communication, 1999).

Prior to entering the mapping phase of its mission, the spacecraft's orbit changed slowly with time and afforded the instruments different views of the planet that also changed with time. When the spacecraft was near apoapse in the AB1 and SPO mission phases, TES observations scanned the instrument field of view across the planet, sensing many combinations of latitude, longitude, and local time in a short period of time. These sequences, which primarily covered the Southern Hemisphere (because apoapse was always in the Southern Hemisphere) are particularly valuable in the present work.

In Figure 1 we show the coverage in several dimensions for a typical slice of data (15°of L_s) from the AB1 and SPO mission phases. Figure 1a shows the coverage as a function of latitude and longitude. From figure 1a, it is apparent that the coverage is generally complete and uniform over these dimensions to near the north pole. Figure 1b shows the same data as a function of latitude and local time. In this representation it is clear that the data north of ~30°S are highly concentrated about one time of day, while south of that they are generally complete and uniformly distributed. This coverage severely hampers our ability to determine the tidal amplitudes for the Northern Hemisphere. However, a similar plot for the mapping mission phase data would have all latitudes having observations at exactly 2 times of day, making the tidal amplitudes significantly harder to determine. Finally, Figure 1c shows a set of cuts in longitude and time of day for nine different latitudes. This plot again shows how the coverage in time of day becomes sparse north of ~30°S. It also shows that where there are observations, they are generally uniformly spaced in longitude versus local time. If there were significant correlations between the longitude of an observation and its local time, it would again be more difficult to separate out the tidal amplitudes from the stationary wave amplitudes.

2.2. TES Retrievals

The TES instrument is a Michelson interferometer, measuring thermal emission between 1600 and 200 cm^{-1} with a resolution of either 5 or 10 cm^{-1}. Using the 15 micron CO_2 absorption band complex, atmospheric temperatures can be retrieved [e.g., *Conrath et al.*, this issue]. While the instrument has the capability of scanning the forward and aft limbs of the planet to increase vertical resolution of the retrievals, we only considered retrievals of the (much more common) near nadir observations. The effective vertical resolution of these near nadir observations is larger than 1/2 of a scale height ($\gtrsim$5 km). The TES team has prepared a data set reporting the atmospheric temperature of each retrieval on a standard pressure grid with a half scale height interval, starting at 6.1 mbar, the reference pressure we use throughout this work (i.e., P_i=6.1 mbar [$\exp(-i/2)$] for $i = 0, 1, \ldots, 8$). The lowest pressure in the grid for these near-nadir observations is 0.11 mbar or an altitude of four scale heights. For pressures lower than this, the information content of the signal is minimal [*Conrath et al.* this issue]. The temperatures are reported for every near nadir observation from the AB1

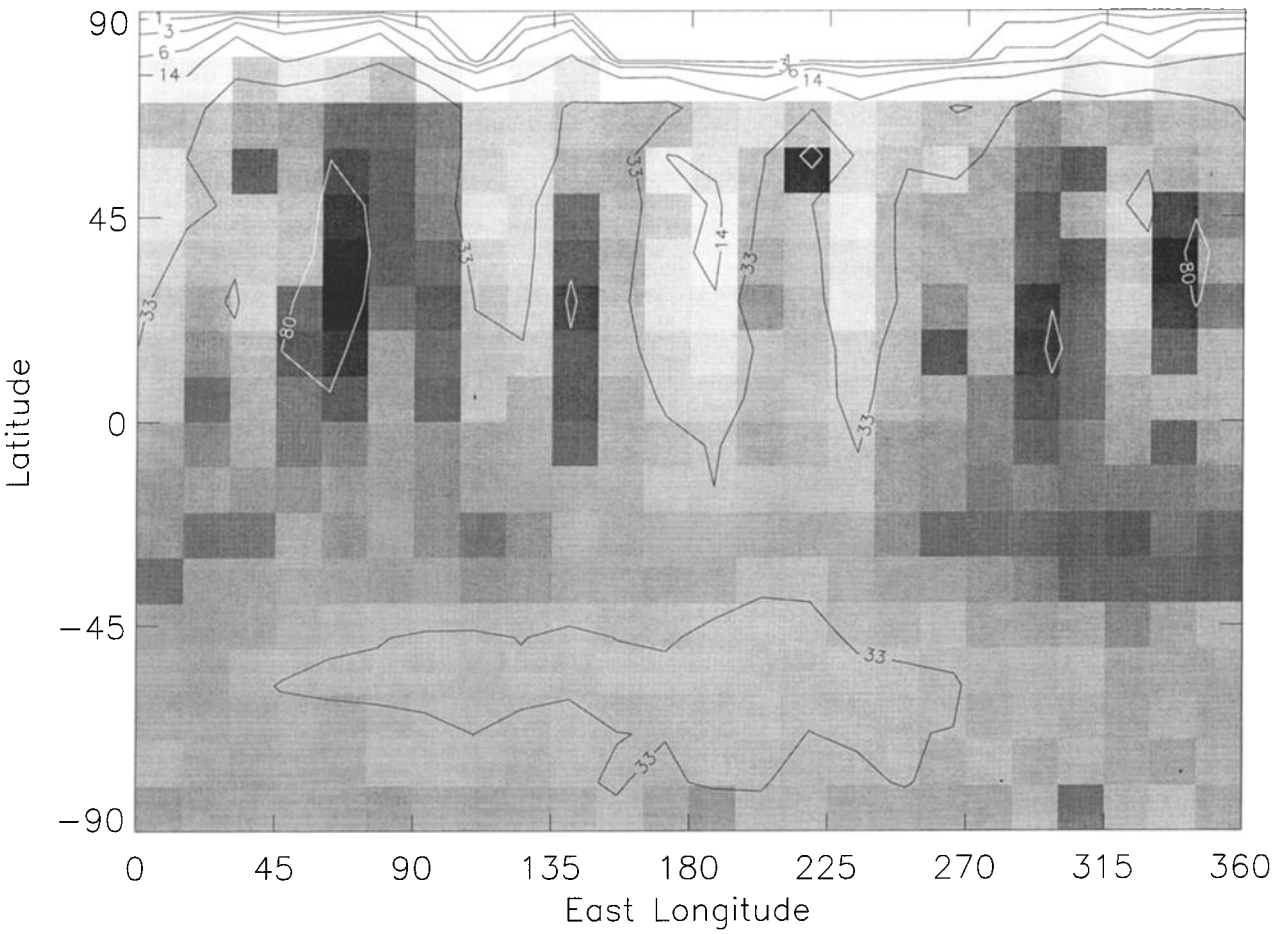

Figure 1. The coverage afforded by the spacecraft during a typical 15°L_s period in the AB1 and SPO mission phases plotted as a function of several different dimensions. (a) The number of observations in each of our bins as a function of latitude versus longitude is shown. Coverage is good and roughly uniform. (b) The coverage as a function of local time versus latitude is given. Note that the coverage in the north is very poor in local time but relatively good and uniform in the south. (c) The coverage for nine different latitude bins as a function of longitude versus local time is shown. Again, note that the north has very poor local time coverage, while the south is more uniform. Furthermore, the observations in the south are roughly uniformly spread over the longitude-local time plane.

and SPO phases of the mission, except at those locations where topography penetrated into the pressure level considered for the region being observed, or the spectrum was corrupted and uninterpretable.

The retrievals of atmospheric temperature from TES spectra are subject to several noise sources. These include instrument noise, errors in the estimated surface pressure, radiometric calibration of the instrument, and assumptions about surface emissivity and atmospheric dust opacity. The magnitudes and behavior of these error sources are such that all retrievals are subject to an error of ~1-2 K. Additionally, the error bars on retrieved temperatures in the lowest scale height are dominated by possible surface pressure errors. The TES retrievals used in this work were performed without the use of the Mars Orbiter Laser Altimeter (MOLA) topography and thus likely have significant errors in the surface pressure assumed for the calculations [*Conrath et al.*, this issue]. For example, a 5% error in the surface pressure can lead to a 1-6 K error in the retrieved temperature for the lowest layer, for surface temperatures of 200-260 K, respectively [*Conrath et al.*, this issue].

3. Modes Considered

This work is focused on the wave modes in Mars' atmosphere that are either constant with time and of integral wave number in longitude (globally coherent stationary waves, including the zonal mean) or varying with a frequency that is an exact multiple of 1 sol^{-1} (solar thermal tides). We also include those tidal modes which are not Sun-fixed but which are expected to be produced by the interaction of the Sun-fixed tides with longitudinal asymmetries in either the forcing or the

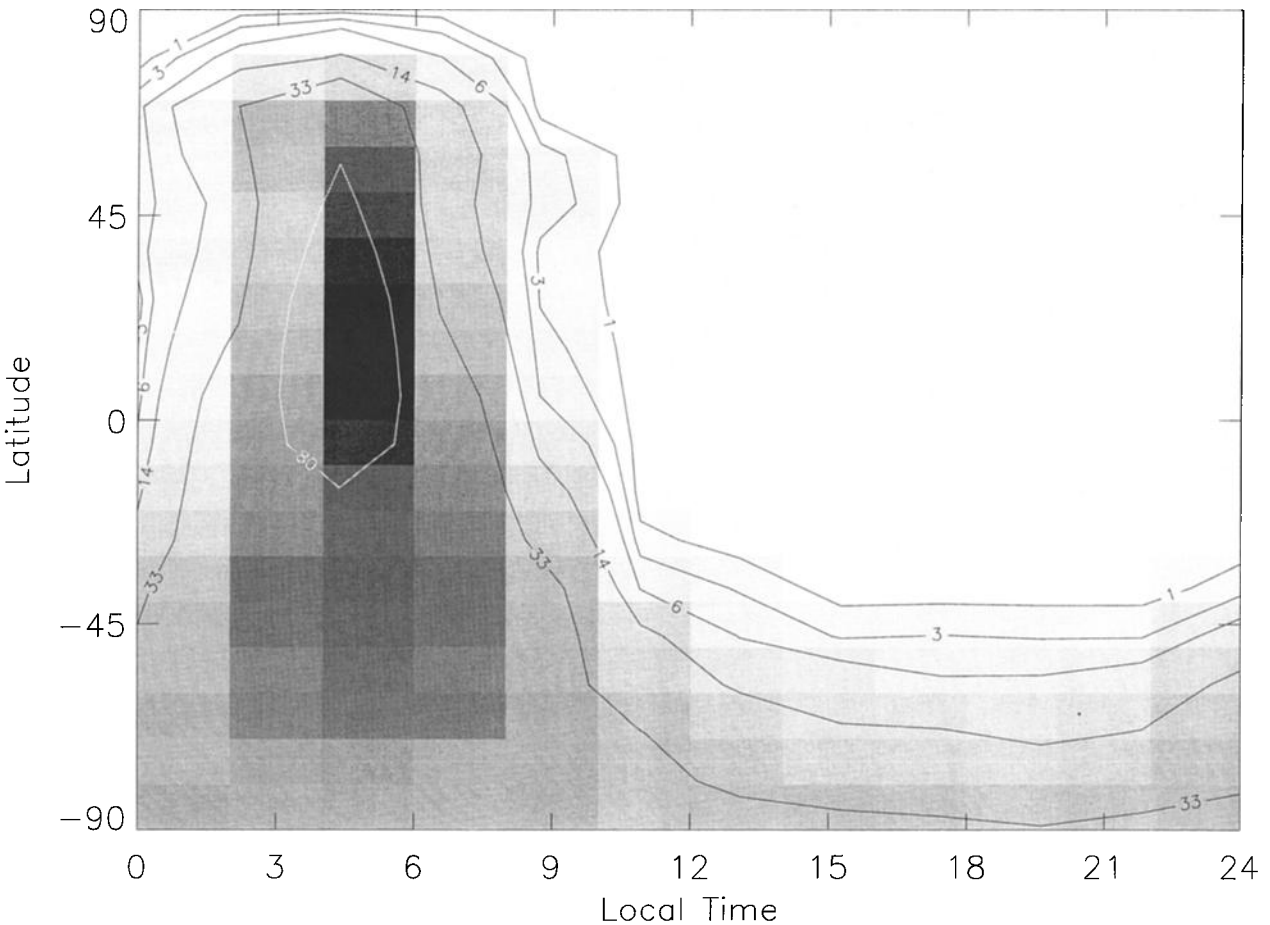

Figure 1. (continued)

topography. Finally, we also included a secular term which accounts for the seasonal drift in the zonal and time of day mean temperatures. Generally, this term was small over the averaging periods; however, it was notably large during one of the dust storms.

We have generally followed the conventions by *Chapman and Lindzen* [1970], except our definition of phase. We can express the perturbation temperature by

$$T = \Re e\{\sum T^{\sigma,s}(\theta,z)e^{i(\sigma t+s\phi)}\} + T^{\text{secular}}(\theta,z)(t-t_0), \quad (1)$$

where T is temperature, θ is latitude, z is altitude, t is time, ϕ is (east) longitude, σ is a wavenumber in time (positive by convention), and s is a zonal wavenumber. $T^{\sigma,s}(\theta,z)$ is the amplitude of a particular wave mode. $T^{\text{secular}}(\theta,z)$ is the amplitude of the secular drift mode, and t_0 is a reference time, the mean value of t for the observations. We define the phase of a mode, ζ using

$$\zeta^{\sigma,s} = \tan^{-1}\frac{\Im m\{T^{\sigma,s}\}}{\Re e\{T^{\sigma,s}\}}. \quad (2)$$

If we wish to limit the modes considered to those mentioned above, this limits the combinations of σ and s allowed. First we consider only globally coherent modes, implying that $s = 0, 1, 2, \ldots$. The stationary modes all have $\sigma = 0$, that is, no time variation. The solar tidal modes have a phase speed equal to that of the sun, $c_{\text{sun}} = -1 = c_{\text{phase}} = -\frac{\sigma}{s}$, and are therefore limited to $s = \sigma$. Finally the tidal modes produced from interactions between the Sun-following tides (of longitudinal wavenumber $s_0 = \sigma$) and longitudinal variations in heating or topography (of longitudinal wavenumber m) can be expressed as the sum of terms with $s = s_0 + m$ and $s = s_0 - m$ [e.g., *Zurek*, 1976; *Conrath*, 1976].

This leaves us with three groups of modes, $\sigma = 0, s = [0, 1, 2, \ldots]$ (the stationary modes); $\sigma = [1, 2, 3, \ldots], s = \sigma$ (the Sun-following tidal modes); and $\sigma = [1, 2, 3, \ldots]$, $s = \sigma \pm m$ for $m = [1, 2, 3, \ldots]$ (the longitudinal variation forced tidal modes), in addition to the secular term. Note that because we only consider integer values of σ, then we can treat time as periodic with period 1 sol (except for with the secular term). Essentially, this just echoes the fact that we are only interested in wave modes that vary repeatably over exactly a sol. The other combinations of s and σ not within these groups represent wave modes that are neither fixed to surface features nor directly forced by the sun. They are the traveling waves that are usually called "weather" by most and will be the subject of our next work with this data set. In fact, to better reveal the "weather,"

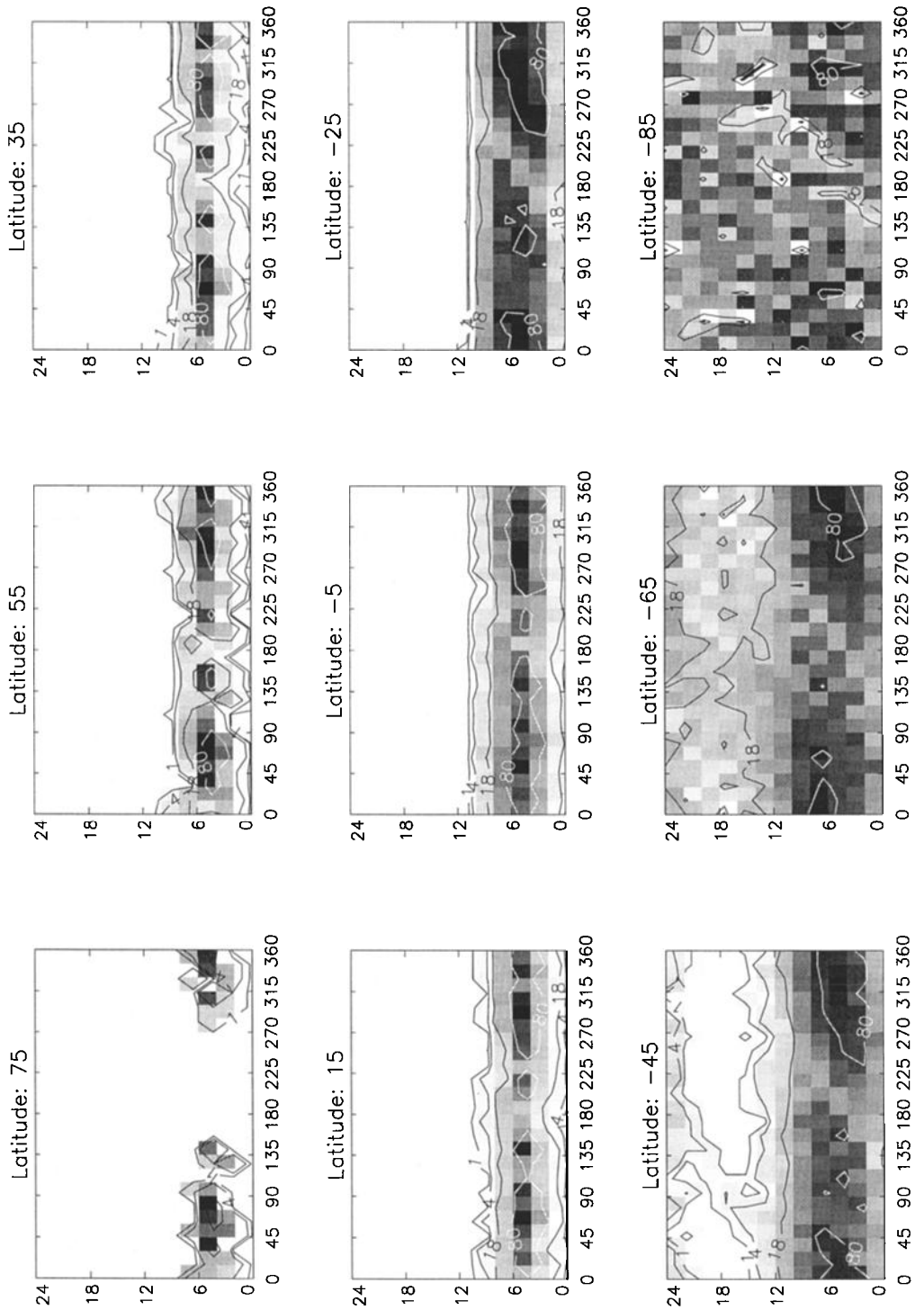

Figure 1. (continued)

we must first isolate the well-defined variations under scrutiny here.

Obviously, there is a limit to how many modes can be fit from a given set of data. We have experimented with fits to $\sigma_{\max} = 3$ and $m_{\max} = 3$ and found that power decreases as the mode frequency increases. Specifically, the modes added by increasing from $\sigma_{\max} = 2$ and $m_{\max} = 2$ to $\sigma_{\max} = 3$ and $m_{\max} = 3$ only explain ~6% more of the power in these types of waves. For comparison, note that we find that the diurnal tide alone accounts for ~70% of the power in these types of waves. Furthermore, the data coverage makes it difficult to reliably retrieve fits for the high-frequency modes. Thus, for this work, we have limited ourselves to $\sigma_{\max} = 2$ and $m_{\max} = 2$, which should contain most of the power in the data set for these types of wave modes.

4. Estimation

4.1. Amplitudes and Phases

To estimate the amplitudes of the different wave modes outlined above, we used a combination of binning and least squares fitting, based on the ideas of *Wu et al.* [1995] (see *Wu et al.* [1995] for more details on the approach). The data set we used from the TES team was already sampled on nine distinct pressure levels, each separated by half a scale height, starting at 6.1 mbar. We kept that vertical sampling in our analysis. We broke the data into L_s blocks of 15°to resolve seasonal and dustiness changes well. In testing this choice of seasonal resolution, for one section ($L_s = 300° - 320°$, which includes a dust storm) we found that $10° L_s$ blocks yielded notably better resolved changes. For that period, we used $10° L_s$ bins. It is important to include a long enough period to give good coverage of longitude and time of day and to average over lower-frequency waves. However, too long an interval will smear out seasonal or other atmospheric behavior changes. It appears that 10°-15°L_s bins were a good compromise for this TES data set.

We chose not to fit spherical harmonics or Hough functions to the data for each L_s and altitude bin. Because of the poor coverage in the north, the global nature of Hough functions would have resulted in poorly constrained fits. Rather, we chose to bin the data further by latitude and then, within each of those bins, fit Fourier series in longitude and time to the data. This proved to be simpler and also allowed us to keep relatively high resolution in the meridional direction, without having to fit to high-order spherical harmonics. We chose 10°bins in latitude, which still afforded good coverage for most latitudes, yet resolved the latitudinal variations well.

Finally, instead of fitting the longitude-time Fourier series directly to all the raw data, we further binned it in the longitude and time dimensions. This allowed us to greatly speed up the fitting process, without sacrificing accuracy. That is, instead of evaluating the Fourier spectrum for every datum, we evaluated it for a limited set of locations in longitude and time, resulting in perhaps a factor of ~16 increase in speed (the median number of observations per bin). We used 24 bins in longitude (15°bins) and 12 bins in time (2 hour bins).

Because our data set is not uniformly sampled in the longitude-time domain, aliasing is a significant problem. This can be seen heuristically in that the different Fourier modes, while orthogonal on a uniformly sampled domain, have significant correlations for our limited and nonuniform sampling. Therefore power in a given mode in the data set will have nonzero convolutions with other modes. This constitutes aliasing, power leaking from one mode into another that is nonnegligibly correlated with the first mode for incomplete sampling.

Periodogram techniques only compute the convolution of the data with a set of modes. The end user then must interpret these convolutions in terms of mode amplitudes while being aware of the possibilities of aliasing. Least squares fitting of the modes to the data goes one step beyond the periodogram techniques, in that minimizing the difference between model and data helps separate those modes with high convolutions with the data into ones that represent real power and ones which are more likely aliased noise. As an example, two modes could show convolutions with the data set that differ by a few percent and are highly correlated. Using a periodogram technique, the end user would have difficulty deciding if both are likely to have power or if one is real and the other aliased. The least squares fitting would use the fact that one mode would likely fit the data better than the other (although only marginally so) and would ascribe the power to the best fitting mode. For this reason, we chose to use least squares fitting of the modes rather than periodogram techniques.

4.2. Error Bars

A least squares fit will return formal error bars to accompany the retrieved parameters. However, the formal error bars only represent how well the model fits the existing data. It includes no estimate of aliasing possibilities. To include this, we modeled the error bars using a Monte Carlo technique. We took the observing pattern for each set of L_s, altitude and latitude bins that we were fitting, and manufactured many sets of synthetic data with 2 K observational errors. Then by examining the standard deviations of the retrieved mode amplitudes, we estimated the combined effects of the noise in the data, as well as the gaps in the coverage contributing to aliasing. This approach is probably effective in estimating the relevant error bars, but it does have shortcomings. Our choice of temperature retrieval observational error is almost certainly an oversimplification. We noted above that the observational error is larger near the surface because of surface radiance, and the poorly known (pre-MOLA) topography. Thus a constant 2 K observational error for all altitudes prob-

ably overestimates the errors at high altitudes and underestimates them at low altitudes. Another shortcoming of this approach is that it only accounts for aliasing among the modes that are being fit. Heuristically, this can be understood in that the least squares fit divides the observed power between the modes being fit. The observational noise, combined with the incomplete observing pattern causes leakage between the modes, or aliasing. Because the power is only divided between the modes being fit, the aliasing is only accounted for between those modes. To minimize this problem, we typically fit out to $s_{\max} = 2$, the results of which suggested that there is significantly less power at higher wavenumbers. Therefore we are likely accounting for most of the power that could be aliasing into the important (low wavenumber) modes.

5. Results

Here we present our results. The format of the presentation is cross sections of mode amplitude and phase as a function of altitude and latitude. We present a set of these cross sections, an individual plot for each L_s bin. The phase (being a circular variable) is represented by color on these plots, with a spectrum that wraps around also in a circular fashion. Amplitude is represented both by contours and also by the saturation of the color, the contours yielding readable values.

Regions that are left blank on these plots were filtered out for one of several reasons. The strongest reason that we left a region blank was due to the least squares fit being ill determined. This typically resulted from there being fewer filled bins (in longitude and time) than the number of modes being fit. The regions affected by this were at all latitudes in the north and near the ground. Another reason that we left regions blank on these plots was that the retrieved amplitude of the mode was less than the estimate of the error bars on that mode. That is, that mode is consistent with a value of zero. The amplitude for the mode that we retrieved in those locations may be correct, but we chose to cut those values from the plot to ensure that the values displayed are significant. This constraint filtered out the results from regions that were just north of the valid results shown in the plots to near the equator. Finally, we did not display values which had error bars associated with them greater than 5 K. This typically cut values which were anomalously high in the retrieval, and only a few scattered locations were effected. Because of these factors, our plots only extend from the south pole to 10°N.

5.1. Zonal Mean, Time Mean: $\sigma = 0, s = 0$

The zonal mean, time mean mode, $\sigma = 0$, $s = 0$ appears in Figure 2. Note that for this mode, phase is undefined, so it appears in black and white. For many values of L_s, we were only able to constrain this mode well as far north as ~20°S. We were also unable to constrain this mode well in the lowest half scale height at any latitudes. There are two gaps ($L_s = 285° - 300°$ and $L_s = 320° - 360°$) in the data set.

This mode is the quantity that is presented in the zonal mean, time mean cross sections, such as by *Conrath et al.* [this issue]. However, the approach used in that and other works simply averages many observations together, ignoring the possibility of aliasing and waves. Our work can be used to estimate the magnitude of these possible effects and thus an estimate of the error bars on those profiles. We carefully computed zonal means using the same subsets of data and the same bin sizes as were used by *Conrath et al.* [this issue] (not shown) and found our results to agree with theirs quite well where we can determine a reliable result. The typical standard deviation of the differences between our results and theirs in the valid regions was ~1 K. This means that the sampling throughout the AB1 and SPO mission phases is uniform enough in longitude and time of day that the simple means of the data are representative of completely and uniformly sampled means. However, keep in mind that this is only true in those regions where we have been able to determine a reliable result, or south of ~20°S. North of this we are not able to estimate the strength of the other modes and can make no estimate as to the accuracy of the simple averages of the data at those latitudes. Using our estimates, error bars of 5 K or more are possible in the zonal averages of *Conrath et al.* [this issue] for the northern latitudes.

The seasonal progression of this mode shows the Southern Hemisphere warming and losing its latitudinal gradient from $L_s = 180° - 255°$. The latitudinal gradient even reverses (warmer at the pole) for $L_s = 255° - 285°$, then returns to being warmer at the equator by $L_s = 30°$. A notable warming occurs from $L_s = 225° - 240°$, coincident with a large dust storm in Noachis [*Smith et al.* this issue]. A smaller but still notable warming also occurs at $L_s = 310° - 320°$, which is also coincident with a smaller dust storm north and northwest of Argyre which started at $L_s = 309°$ [*Smith et al.* this issue]. Still further pursuing the similarities between the observed dust opacity from *Smith et al.* [this issue] and these results, we see that the cooler Southern Hemisphere temperatures from $L_s = 0° - 30°$ (compared to similar solar input at $L_s = 180° - 195°$) are again consistent with the reduced dust opacity observed at that time.

5.2. Zonal Mean, Time Mean Secular Trend: $\sigma = 0$, $s = 0$

We also fit a secular trend to the zonal and time mean temperature distribution, which is depicted in Figure 3. This mode is important to fit because it has significant amplitude, and without including it in the fit, it could easily alias into other modes. The structure of this mode is enlightening as well. It mainly echoes the seasonal changes noted in the zonal and time mean term above, that of slow warming in the south during south-

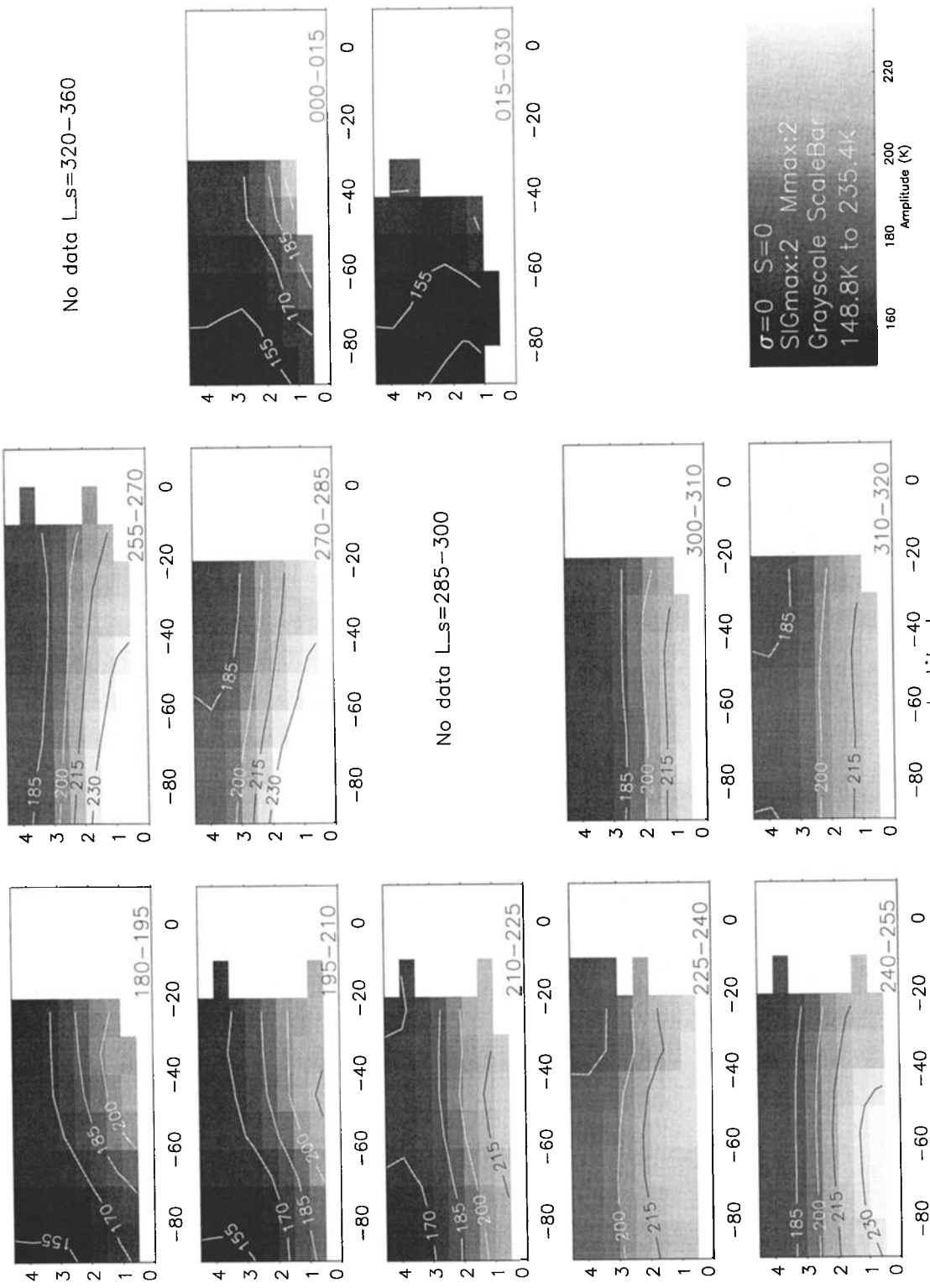

Figure 2. The amplitude of the zonal and time mean mode, $\sigma = 0$, $s = 0$. Each separate plot is for one band of L_s, indicated on the lower right of each plot. Each plot is then of latitude versus altitude (in scale heights above 6.1 mbar), with the amplitude in Kelvin. A scale bar is on the lower right. Blank spaces are regions that the data would not allow reliable determination of the amplitude of this mode. Note the seasonal changes as the warmest locations follow the Sun north and south.

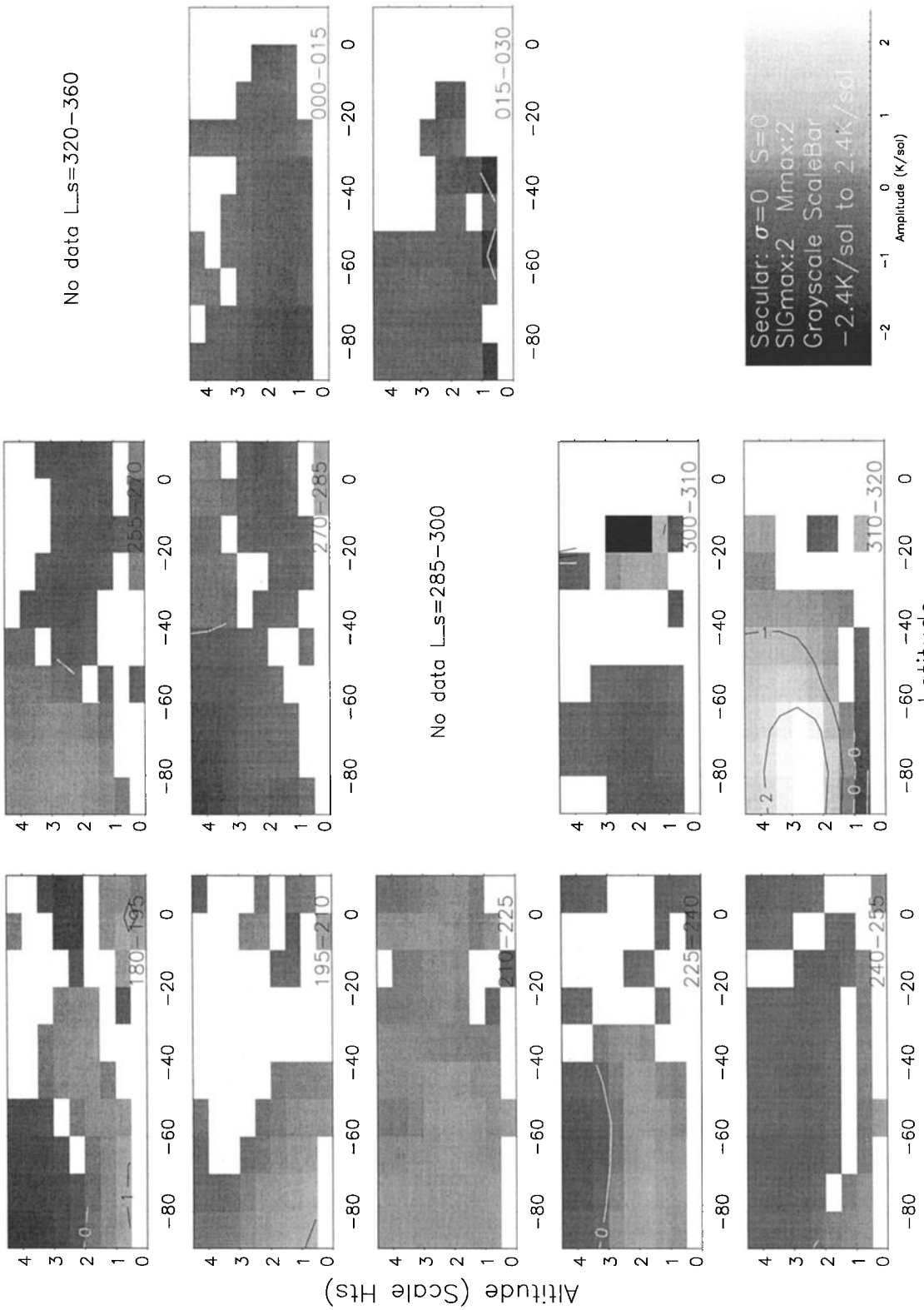

Figure 3. The amplitude of the secular change of the zonal and time mean mode, $\sigma = 0$, $s = 0$. The format of this plot is the same as that for Figure 2, except that the units are K/sol. Note the strong warming during the dust storm from $L_s = 310° - 320°$ but the absence of such strong warming during the larger dust storm from $L_s = 225° - 240°$.

ern spring and slow cooling in the south during southern fall. However, it also shows a very large warming (2.4 K/sol) in the high southern latitudes, centered at ~2.5 scale heights altitude during the smaller dust storm near Argyre ($L_s = 310° - 320°$). There is also a hint of an elevated heating rate during the Noachis dust storm ($L_s = 225° - 240°$), but this is much more subtle than that evident during the smaller $L_s = 310° - 320°$ storm. This is even more surprising in light of the fact that the seasonal temperature trends are working against the warming at $L_s = 310° - 320°$, while they would enhance that during $L_s = 225° - 240°$. Perhaps this is indicating something very different about the dust distribution or the resulting diabatic circulation in these two dust storms.

5.3. Sun-Synchronous Tides

5.3.1. Diurnal Tide: $\sigma = 1, s = 1$. Plate 1 shows the amplitude and phase of the sun synchronous, diurnal tide. More locations are left blank on these plots than on those for the zonal and time of day mean mode because the amplitudes of this mode are much smaller and more often less than the error bars at a given location. However, throughout much of the Southern Hemisphere, the diurnal tide is well resolved by the TES data, with amplitudes of order 4 K.

In the southern extratropics, for most of the L_s values we cover, we generally see a constant phase of ~90°(maximum at about 1800 LT, green in Plate 1). In that latitude range, this mode is expected to lag the sun and not propagate vertically, as we observe. There is a significant departure from this behavior from $L_s = 255° - 285°$, poleward of ~50°S and above two scale heights. In this region, we see the amplitude significantly decrease (down to ~2 K), and the phase change to leading the sun by ~90°(maximum at about 0600 LT, purple in Plate 1). Because the amplitude decreases in that region, it is conceivable that our retrieval of phase is less significant even though it exceeds the associated error bars. However, Figure 4 demonstrates that this is not the case. Figure 4 shows normalized temperature variations about their means as a function of altitude versus local time, for four 10°latitude bins near the south pole for $L_s = 240° - 255°$ and $L_s = 270° - 285°$. The phase reversal for the southernmost 30°of latitude is evident for the $L_s = 270° - 285°$ plots, while it is clearly absent from the earlier ones. Shown in this manner, it is evident that this phase reversal is a significant result and not an artifact of the relatively small amplitude in that region. We will return to this topic in section 6.

Nearer the equator, the other structure we see in this mode's phase is what appears to be a phase advance (maxima occurring earlier in the day, color changing from red to green in Plate 1) with height near the bottom, and a phase regression (maxima occurring later in the day, color changing from green to red in Plate 1) with height near the top of our domain, although in the tropics the poor coverage makes this somewhat ambiguous. It is perhaps most clearly evident in Figure 4 for $L_s = 240°$ and the two most equatorward latitudes. This phenomenon occurs roughly equatorward of 50°S, with the strongest expression centered around $L_s = 270°$, southern summer. If the heating is all deposited near the surface, tidal theory predicts a phase advance (maxima occurring earlier in the day) with height at all altitudes near the equator and a vertical wavelength of ~35 km [e.g.,*Zurek*, 1976]. This is consistent with the behavior we see from the bottom to the middle of our domain but not with that near the top. Perhaps this behavior at high altitude is indicative of heating significantly removed from the surface. Furthermore, the apparent phase advance with height near the bottom of the domain starts with a local maximum near midnight, directly out of phase with the sun. While this can not be a direct leakage of surface radiance into this level of the retrieval (because it is 180°out of phase), it may still be an artifact of the retrieval process. Surface effects have been identified as a possible source of error by the TES team, but the exact magnitude is difficult to quantify. This low-altitude phase advance with height may also be a real phenomenon. We will return to this topic in section 6.

There are two aspects of this mode in the latitudes in which it vertically propagates which are interesting. The first is that this region extends to ~60°S for some L_s values. Simple tidal theory predicts that vertical propagation stops at 30°S, although modeling work [*Wilson and Hamilton*, 1996] shows it extending somewhat poleward of 30°, particularly into the winter hemisphere due to the strong westerlies there. The second aspect of interest is that the amplitude does not seem to grow with height inversely with the density to maintain a constant energy flux through the domain. Instead, the amplitude is roughly constant with height near the tropics, perhaps decreasing with height at more values of L_s than increasing. This is probably indicative of either the distribution of forcing for this mode or conversely its damping. Both of these aspects of this dominant tidal mode are intriguing and need further exploration.

Outside of the latitude band where the mode appears to propagate vertically, it is interesting to note the distribution of amplitude as a function of location and season. The amplitude is very high at the same locations and the same season as the large Noachis dust storm near $L_s = 225° - 240°$. This is expected, as a large dust opacity should indicate a strong coupling between the solar forcing and the atmosphere's thermal response. This range of L_s in fact exhibits amplitudes in excess of 8 K as high as four scale heights above the surface, perhaps suggesting that the dust is well mixed very high into the atmosphere. The amplitude decreases again as the seasons advance, in concert with the dust opacity, until at $L_s = 310° - 320°$ it shows amplitude > 8 K

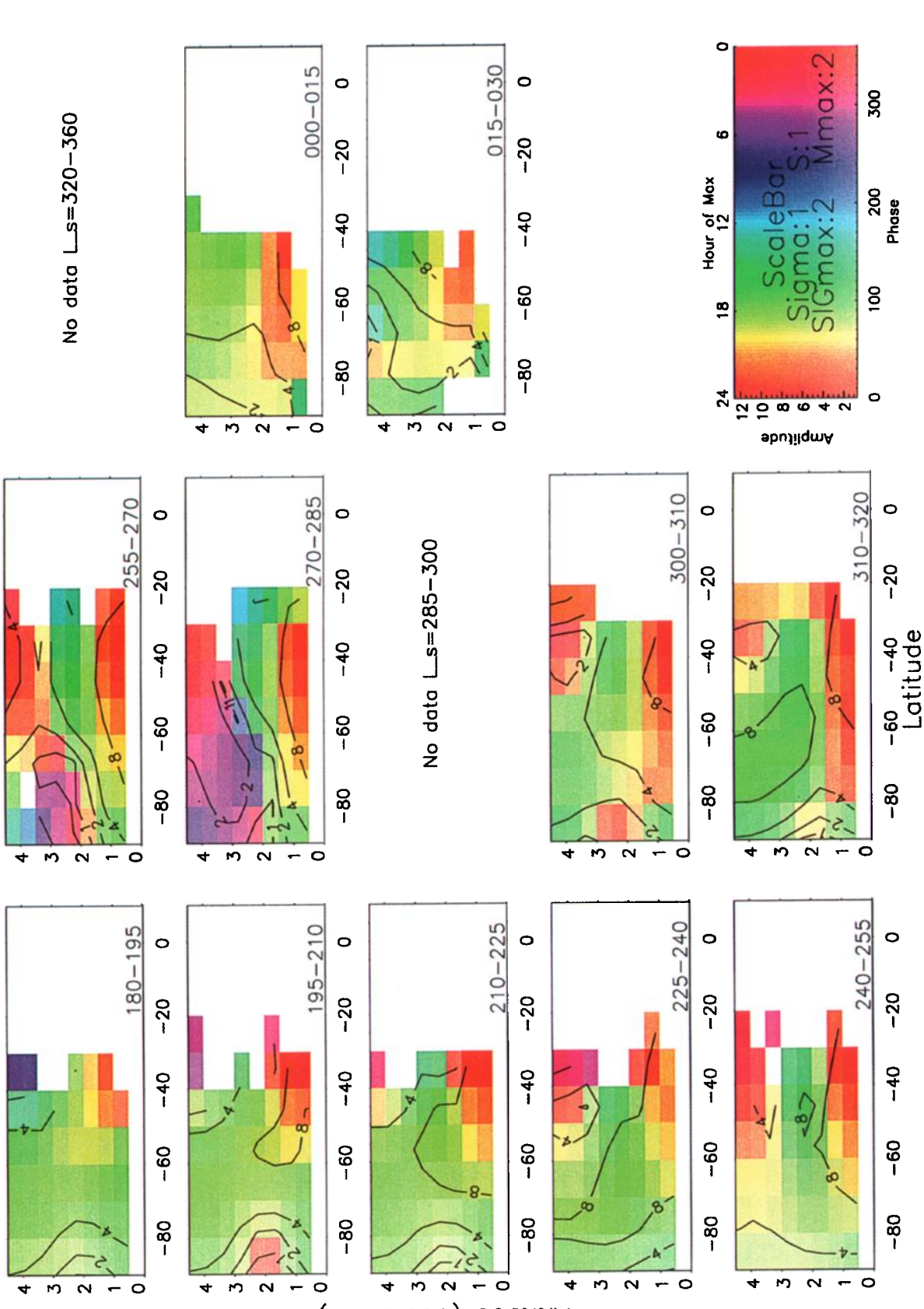

Plate 1. The amplitude (contours and color saturation) and phase (color) of the sunsynchronous, diurnal tide mode $\sigma = 1$, $s = 1$. The structure of this plot is the same as Figures 2 and 3, with the addition of phase information. The time of temperature maximum is also indicated on the color bar. Note the significant amplitude, especially during the dust storms from $L_s = 225° - 240°$ and $L_s = 310° - 320°$. Note also the apparent phase reversal in the south two scale heights up from $L_s = 255° - 285°$. Also puzzling is the phase of the large amplitude tide near 40°S and 1/2 scale height in altitude. It has a maximum near local midnight.

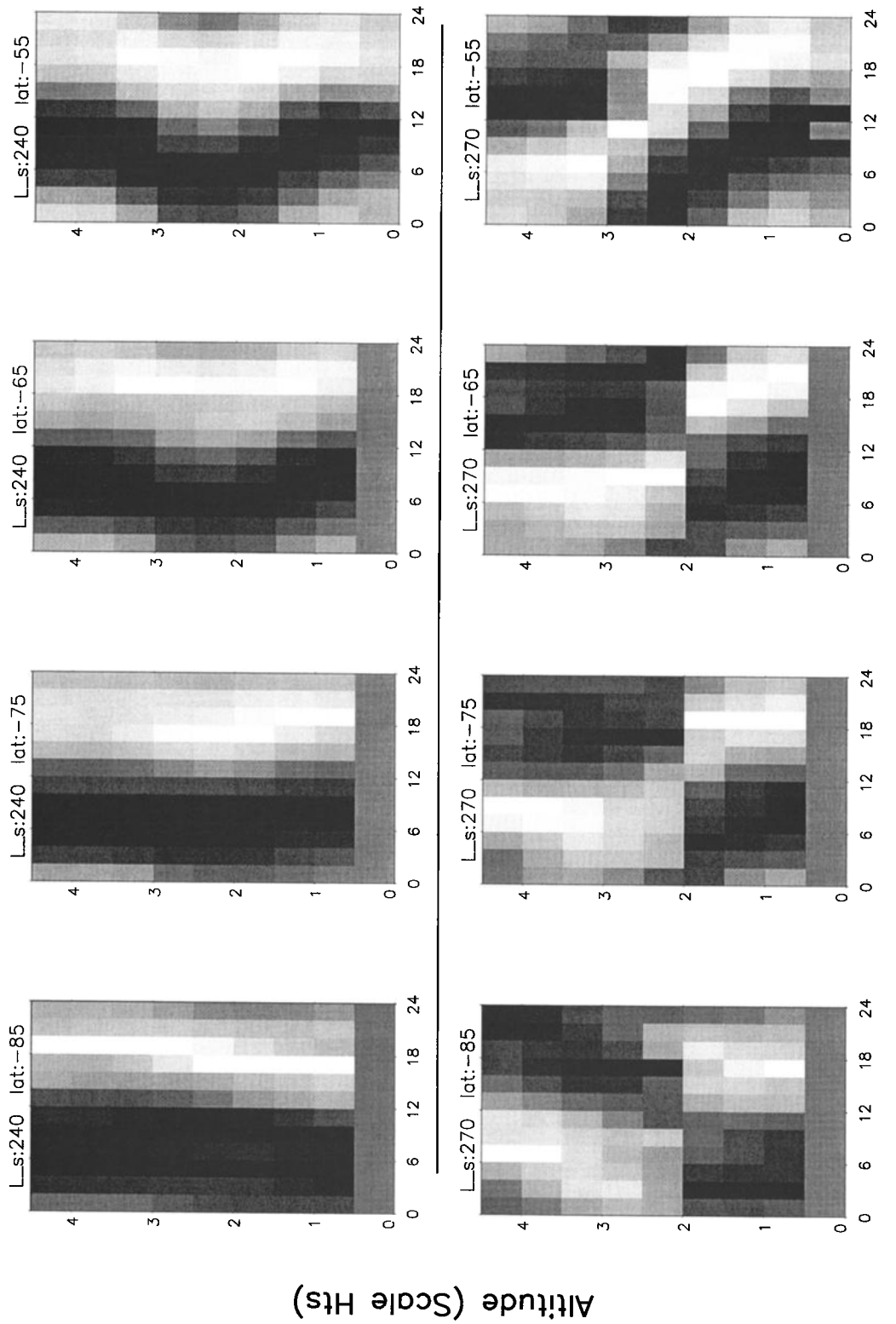

Figure 4. Normalized temperature variations as a function of local time versus altitude for two seasonal cuts and four latitude bins. The local time mean temperatures at each altitude, latitude and season in this plot were subtracted, leaving only the local time variations. These variations were then normalized by their maxima. This highlights the phase behavior of the tides as a function of altitude and latitude. Of particular note is the phase reversal that appears for the southernmost 30° of latitude for $L_s = 270° - 285°$ at two scale heights up. A phase reversal like this is not seen in the other TES data analyzed in this work.

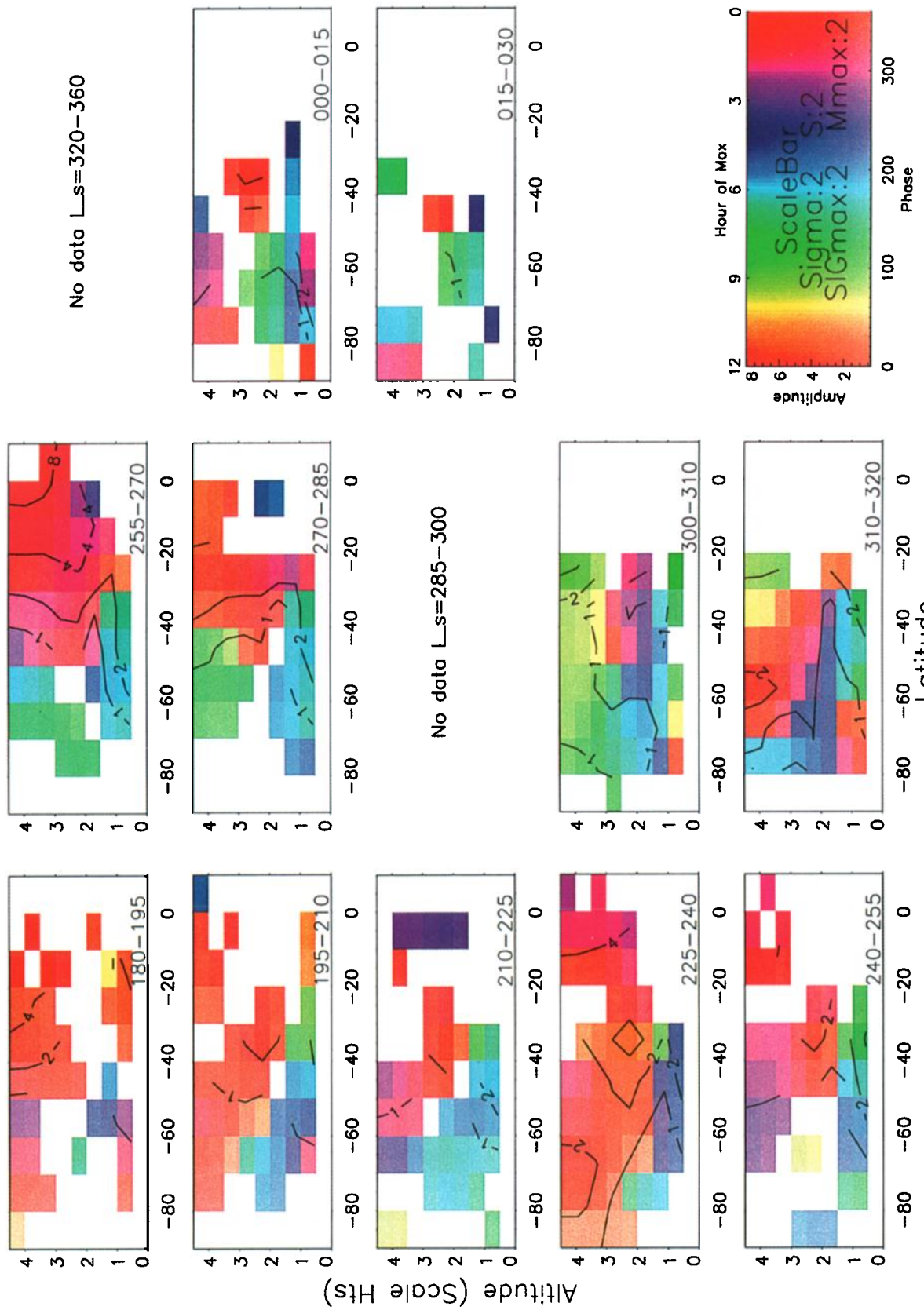

Plate 2. The amplitude and phase of the semidiurnal tide, $\sigma = 2$, $s = 2$. The structure of this plot is the same as that of Plate 1. Note the smaller amplitudes of this mode and how they grow toward the north and with altitude near the equator.

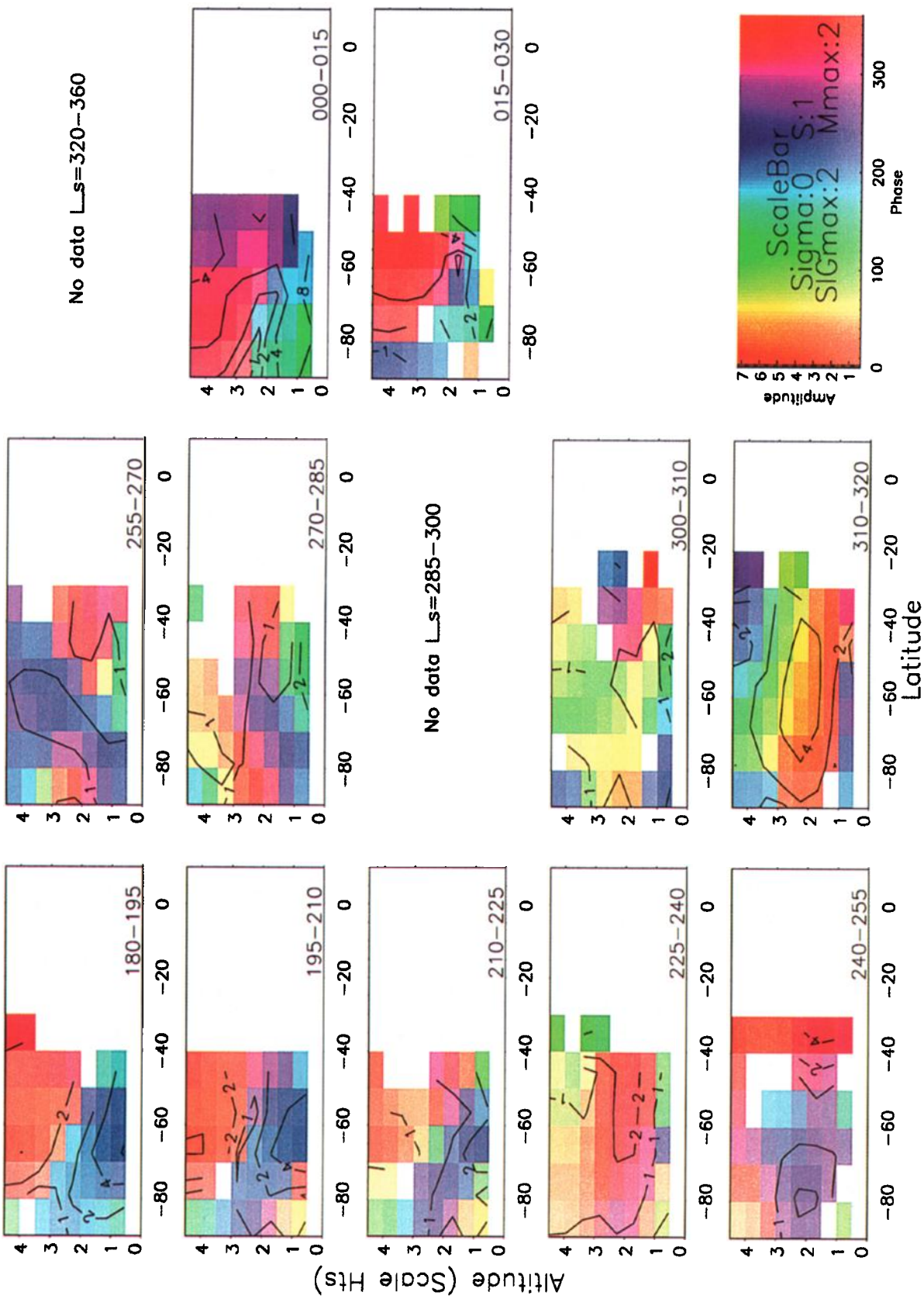

Plate 3. The amplitude and phase of the mode 1 stationary wave, $\sigma = 0$, $s = 1$. The format of this plot is the same as Plates 1 and 2. Note the large amplitude and markedly different phase during the $L_s = 310° - 320°$ dust storm.

over a broad region of the southern extratropics, two or more scale heights up. This period once again coincides with one of the other significant dust storms already identified by TES retrievals [*Smith et al.* this issue]. This dust storm appears to excite a high-amplitude diurnal tide even higher than that during the Noachis dust storm, perhaps suggesting that the dust was more concentrated at altitude than below.

Wilson and Hamilton [1996] present model simulations which we can directly compare with one of these seasonal plots. *Wilson and Hamilton* [1996, Figure 16a] show a cross section like ours for $L_s = 270°$ and low dustiness. The agreement in amplitude is generally good. We find a large amplitude near the surface, perhaps 8 K or more below one scale height. Their results indicate an amplitude of roughly 5 K or more in that region, then decreasing to a minimum of ~1 K near three scale heights and increasing again above that. This is very similar to our results, where we see a minimum amplitude of ~1 K between two and three scale heights. *Wilson and Hamilton* [1996, Figure 16d] show the phase of the zonal wind oscillation being essentially constant from 30°S poleward. This is the time in which we find the phase reversal with height at two scale heights in the temperature signal. While Wilson and Hamilton's plot is for zonal wind and ours is for temperature, there is an apparent discrepancy here between their modeling and our results for this particular season. However, in general for other values of L_s, our results agree with the simulations of Wilson and Hamilton (and with theory) and show no vertical phase propagation of the diurnal tide far outside of the tropics.

5.3.2. Semidiurnal Tide: $\sigma = 2, s = 2$. This mode, the semidiurnal tide shown in Plate 2, is interesting in that it is typically much smaller in amplitude than might be expected. We were able to reliably determine the amplitude of this mode for ~50% of the altitudes and latitudes in the Southern Hemisphere. The regions where we could not determine the amplitude reliably were either too sparsely observed or the amplitude was too small to distinguish it from noise. Throughout the southern extratropics, a typical amplitude of this mode is ~1 K. Within the tropics the amplitude is larger, reaching ~8 K three scale heights above the equator. The amplitude is greatest over the equator, and it could be growing with height as quickly as a factor of 2 for each one to two scale heights. This is notably similar to the $\rho^{-1/2}$ that is predicted for conservation of energy flux for a vertically propagating mode.

We know of no published estimates of the latitude-altitude behavior of the semidiurnal tide of Mars. The Viking landers yielded good data sets of the semidiurnal pressure variations with time. These showed significant semidiurnal amplitudes, strongly increasing their amplitudes during global dust storms [e.g., *Leovy and Zurek*, 1979]. While the relationship of surface pressure amplitude to temperature perturbation amplitudes is not straightforward, the simplest expectation would be that the semidiurnal mode might be comparable to the diurnal mode, especially during dust storms. This appears to not be the case from the present analysis, with the typical amplitude of the diurnal mode being of order 5 K in the southern extratropics, while that of the semidiurnal mode is ~1 K. Nevertheless, this is not inconsistent with observations of large semidiurnal surface pressure signals, as the long vertical wavelength of the semidiurnal mode helps enhance its surface pressure signal over that of the diurnal mode (with its relatively short vertical wavelength).

5.4. Stationary Waves

The stationary wave modes have no time of day variation or $\sigma = 0$. We fit the $s = 1$ and $s = 2$ modes to the data. The $s = 1$ mode, shown in Plate 3, has a typical amplitude throughout the Southern Hemisphere of ~2 K, with some locations clearly exceeding 4 K, perhaps a few as high as 8 K. The spatial structure of the amplitude is difficult to connect with any simple idea, but its seasonal variation shows an obvious correlation with the smaller $L_s = 310° - 320°$ dust storm. During this time, the amplitude of this mode is 4 K or more from 40°S to 80°S, centered at two scale heights of altitude, about 4 times the amplitude in those regions from just 10°of L_s earlier. There is also some hint that this mode's amplitude is enhanced during the Noachis dust storm but perhaps only by a factor of 2 or less. During the $L_s = 310° - 320°$ dust storm, the phase of this mode is also anomalous and consistent throughout the region with enhanced amplitude.

Smith et al. [this issue] present maps of dust opacity during both of these dust storms. Their results show that the zonal distribution of dust in the Noachis dust storm is roughly uniform poleward of 40°S, while the $L_s = 310° - 320°$ storm is almost completely contained within one quadrant of longitude in the Southern Hemisphere. It is quite likely that this difference in the longitudinal distribution of dust in these two storms can explain the differences observed in their stationary wave amplitudes. This invites further study into the specifics of the dust heating and the generation of these stationary wave modes.

Hollingsworth and Barnes [1996] and *Nayvelt et al.* [1997] both modeled stationary waves in Mars atmosphere. In agreement with our results, they both found that the Southern Hemisphere is dominated by the $s = 1$ mode. We have not displayed the $s = 2$ mode, as its amplitude is typically < 1 K throughout the region where we can retrieve it. The two modeling works suggest that the $s = 2$ mode is more powerful in the Northern Hemisphere, which is not accessible with this subset of data. *Banfield et al.* [1996] reported stationary waves from an analysis of IRTM T15, but their results regarding the mean state are likely corrupted by surface radiance [*Wilson and Richardson*, 2000].

5.5. Topography-Coupled Tidal Modes

The modes which arise from the interaction between the sun-fixed tidal modes and longitudinal asymmetries (e.g., topography) were also simultaneously fit in this study. In general, these modes are significantly smaller than those discussed above and do not present any clear spatial structures. Because of this, we have not graphically presented any of them here. The largest of these modes in our results for the Southern Hemisphere was the $\sigma = 1$, $s = -1$ mode, which we found to have an amplitude of ~1.5 K, with larger values starting to show up in the northernmost limits of our retrieval (i.e., ~25°S). These northernmost values have the largest error bars, but values of 2-4 K repeatably appear near 25°S. This $\sigma = 1$, $s = -1$ mode propagates eastward at the same speed as the sun moves westward. It includes the eastward propagating diurnal Kelvin mode of previous works [e.g., *Zurek*, 1976] which, unlike our fits, has a well-defined latitudinal structure, confined to the tropics.

The next smaller mode in this group is the $\sigma = 1$, $s = 0$ mode. This mode has a period of 1 sol but no longitudinal variations, essentially a pulsing of the atmosphere, with the same phase of oscillation at all longitudes. Typical Southern Hemisphere extratropics values for this mode are ~1 K, again with indications that the amplitude increases to the north starting around 25°S. This mode also clearly shows an increase in amplitude during the $L_s = 310° - 320°$ dust storm, with amplitudes throughout the southern extratropics of ~2 K, and growing to nearly 4 K above three scale heights near the South Pole. Interestingly, this mode shows no appreciable change during the Noachis dust storm.

Similar behavior is seen in the $\sigma = 2$, $s = 0$ mode, which has a period of one half of a sol and again no longitudinal variations. Typical southern extratropical amplitudes are ~1 K, again increasing to the north beyond ~25°S. This mode also shows a strong increase in amplitude during the $L_s = 310° - 320°$ dust storm, with amplitudes of ~2 K typical throughout the south, and amplitudes exceeding 4 K over two scale heights near the South Pole.

The remaining five modes we fit (i.e., ($\sigma = 1$, $s = 2$), ($\sigma = 1$, $s = 3$), ($\sigma = 2$, $s = 1$), ($\sigma = 2$, $s = 3$), ($\sigma = 2$, $s = 4$)) were all typically less than or on the order of 1 K throughout the southern extratropics, but they all also suggested larger amplitudes to the north.

Wilson and Hamilton [1996] discuss the importance of these modes and present some model calculations suggesting that many of them probably occur in Mars' atmosphere. They suggest that the $\sigma = 1$, $s = -1$ and $\sigma = 2$, $s = -2$ modes may be the strongest of this class of wave at many times of year. They present a plot [*Wilson and Hamilton*, 1996, Figure 17a] of the temperature amplitude cross section of the $\sigma = 1$, $s = -1$ mode which compares very favorably with our results. It shows an amplitude of ~1 K throughout the southern extratropics, with amplitudes increasing into the Northern Hemisphere. Aside from this, we know of no other yet published model runs with which to compare these results.

6. Discussion

These results, extracted from the AB1 and SPO TES data, should provide strong constraints for the numerous atmospheric models that the community now has. Additionally, they may be used to try to infer details of the state of Mars atmosphere. We expect that tidal and stationary wave models will be applied to these data, and estimates of the distribution of forcing and dissipation will be sharpened.

In this work, we identified two puzzling details of the observations that we will explore. The first was the apparent phase reversal of the diurnal tide from $L_s = 255° - 285°$ above two scale heights, south of ~60°S (see Plate 1). We do not have an explanation for this phenomenon; however, we have considered the possibility that it is evidence of a critical layer. If the winds at this height were strong enough easterlies (westward) to match the phase speed of the sun, it is possible that the expression of the tide might show a phase reversal and an amplitude decrease above the critical layer, matching the observations. The thermal winds can be inferred from the zonal and time mean temperature fields, except for the addition of the winds at the surface. Using the thermal winds from *Conrath et al.* [this issue], we can infer what surface wind speeds would be required to produce this critical layer. Near the pole, the winds are very modest, 10 m/s at 85°S. Further north, this hypothesis becomes more unlikely. At 75°S a surface wind of 45 m/s is required, and at 65°S a surface wind of 70 m/s is required. Therefore we find this hypothesis highly unlikely to be correct (without widespread dust storms evident at that time, which was not the case) and leave this phenomenon unexplained.

The second phenomena that we noted was also in the diurnal tide mode. We noted that this mode's phase 1/2 scale height above the surface was 180°out of phase with the Sun (see Plate 1). It shows a temperature maximum near local midnight. Linear tidal theory suggests that an atmosphere heated from below should show a phase advance (temperature maxima moving toward earlier local times) as one moves up above the surface, with the lowest levels having a maximum just after local noon, since that is where and when the energy is deposited. We mentioned above that it is possible that this is an artifact of the retrieval process being corrupted by surface radiance. However, it may be a real phenomenon. The southernmost latitude at which we see the phase advance with height appears to be moderately well correlated with the progression of the subsolar latitude through the seasons. However,

the strength of this effect does not seem well correlated with dust opacity. For example, the dust opacity was highest from $L_s = 225° - 240°$, yet during this time we observe no significant phase advance with height at the bottom of our domain and near the equator.

It is possible that this phenomenon can be explained by convective overshoot. Near midday, particularly at the subsolar latitudes, the martian boundary layer is heated very strongly. This raises the possibility that convective plumes could penetrate significantly into the stable atmosphere above the convecting boundary layer. This would effectively cool this layer (which is necessarily warmer than an adiabat from the surface). The cooling would be strongest when the boundary layer is heated most strongly, near local noon, precisely what our analysis shows. Thus it is possible that we are seeing this convective overshoot follow the subsolar latitude around the southern summer and affect the atmospheric layer between 1/2 and 1 scale height above the surface (5-10 km), almost reversing the apparent phase of the diurnal tide. Confirmation of this may exist in lander temperature entry profiles, or radio occultation profiles, but is probably best observed by upward looking infrared sounding [*Smith et al.*, 1996]. Its potential implications are also unexplored.

7. Summary

We have determined the amplitude and phase of wave modes in the Martian atmosphere based on TES observations of atmospheric temperatures from the AB1 and SPO MGS data. The amplitudes and phases of the diurnal and semidiurnal tides, the first few (gravest) stationary waves and a few modes which are couplings between sun-fixed tides and topography are included. Estimates of the zonal and time of day mean temperature meridional cross sections and their rates of change finish the modes considered.

The zonal and time of day mean temperature meridional cross sections agree with those of *Conrath et al.* [this issue] to within 1 K where we can reliably retrieve this mode (90°S to ~20°S). Outside of this region, potential errors due to the simple averaging employed by *Conrath et al.* [this issue] can not be estimated. Heating rates of up to 2.4 K/sol were observed around three scale heights above 60°S-90°S during the $L_s = 310° - 320°$ dust storm. Diurnal tide amplitudes of > 8 K were observed during the Noachis and $L_s = 310° - 320°$ dust storms. From $L_s = 255° - 285°$ an unexplained phase reversal at two scale heights was observed in the diurnal tide from 60°S-80°S. Convective penetration above the unstable boundary layer may explain anomalous (180°out of phase with the sun) diurnal tide phases between 0.5 and 1 scale height above the latitudes around the subsolar point. Semidiurnal tides are of order 2 K throughout the southern extratropics. Stationary wave $\sigma = 0$, $s = 1$ was observed with amplitude 1-4 K in the southern extratropics. Topographically coupled tide modes were also quantified.

References

Banfield, D., A. D. Toigo, A. P. Ingersoll, and D. A. Paige, Martian weather correlation length scales, *Icarus, 119,* 130-143, 1996.

Chapman, S. and R. S. Lindzen, *Atmospheric Tides,* 200pp., Gordon and Breach, Newark, N.J., 1970.

Conrath, B. J., Influence of planetary-scale topography on the diurnal thermal tide during the 1971 Martian dust storm, *J. Atmos. Sci., 33,* 2430-2439, 1976.

Conrath, B. J., Planetary-scale wave structure in the Martian atmosphere, *Icarus, 48,* 246-255, 1981.

Conrath, B. J., J. C. Pearl, M. D. Smith, W. C. Maguire, S. Dason, M. S. Kaelberer, and P. R. Christensen, 1999, Mars Global Surveyor thermal emission spectrometer (TES) observations: Atmospheric temperatures during Aerobraking and science phasing, *J. Geophys. Res.,* this issue.

Hollingsworth, J. L., and J. R. Barnes, Forced stationary planetary waves in Mars's winter atmosphere, *J. Atmos. Sci., 53,* 428-448, 1996.

Leovy, C. B., and R. W. Zurek, Thermal tides and Martian dust storms: Direct evidence for coupling, *J. Geophys. Res., 84,* 2956-2968, 1979.

Nayvelt, L., P. J. Gierasch, and K. H. Cook, Modeling and observations of Martian stationary waves, *J. Atmos. Sci., 54,* 986-1013, 1997.

Pirraglia, J. A., and B. J. Conrath, Martian tidal pressure and wind fields obtained from the Mariner 9 infrared spectroscopy experiment, *J. Atmos. Sci., 31,* 318-329, 1974.

Smith, M. D., B. J. Conrath, J. C. Pearl, and E. A. Ustinov, Retrieval of atmospheric temperatures in the Martian planetary boundary layer using upward-looking infrared spectra, *Icarus, 124,* 586-597, 1996.

Smith, M. D., B. J. Conrath, J. C. Pearl, and P. R. Christensen, 1999, Mars Global Surveyor thermal emission spectrometer (TES) observations of dust opacity during aerobraking and science phasing, *J. Geophys. Res.,* this issue.

Wilson, R. J., and K. Hamilton, Comprehensive model simulation of thermal tides in the Martian atmosphere, *J. Atmos. Sci., 53,* 1290-1326, 1996.

Wilson, R. J., and M. I. Richardson, The Martian atmosphere during the Viking Mission, 1: Infrared measurements of atmospheric temperatures revisited, *Icarus,* in press, 2000.

Wu, D. L., P. B. Hays, and W. R. Skinner, A least squares method for spectral analysis of space-time series, *J. Atmos. Sci., 52,* 3501-3511, 1995.

Zurek, R. W., Diurnal tide in the Martian atmosphere, *J. Atmos. Sci., 33,* 321-337, 1976.

D. Banfield and B. J. Conrath, Department of Astronomy, Cornell University, 420 Space Sciences, Ithaca, NY 14853. (e-mail: banfield@astrosun.tn.cornell.edu)

P. Christensen, Department of Geology, Arizona State University, Box 871404, Tempe, AZ 85287.

J. C. Pearl and M. D. Smith, NASA/Goddard Space Flight Center, Code 690, Greenbelt, MD 20771.

(Received August 11, 1999; revised December 16, 1999; accepted January 4, 2000.)